Science of the Total Environment 1002 (2025) 180529

Contents lists available at ScienceDirect

Science of the Total Environment

journal homepage: www.elsevier.com/locate/scitotenv

Algae-paper integrated sensor for bisphenol determination in zebrafish embryos

Filippo Silveri [a], Flavio Della Pelle [a,*], Carmine Merola [a], Annalisa Scroccarello [a], Fabio Trabucco [a], Michele Amorena [a], Enrico Cozzoni [b], Rocco Cancelliere [c], Laura Micheli [d], Dario Compagnone [a,*]

[a] Department of Bioscience and Technology for Food, Agriculture and Environment, University of Teramo, Campus "Aurelio Saliceti" Via R. Balzarini 1, 64100, Teramo, Italy
[b] "TheLAB", Via Alvaneto 44/A, 62026, San Ginesio, MC, Italy
[c] ENEA, Technologies and Devices for Electrochemical Storage (TERIN-DEC-ACEL), Rome, 00123, Italy
[d] Department of Chemical Science and Technologies, University of Rome Tor Vergata, Via Della Ricerca Scientifica 1, 00133, Rome, Italy

HIGHLIGHTS

- Algae-paper sensors are proposed to determine bisphenol A in Zebrafish model (*Z*-EBs).
- Sensors were manufactured in series via a smart lab-made stencil printing approach.
- Sensor exploitability was demonstrated in Z-EBs exposed to bisphenol A (BPA).
- Algae sensors allow BPA determination in culture medium and zebrafish embryos.
- Algae sensors allow discriminating sub-lethal BPA levels.

GRAPHICAL ABSTRACT

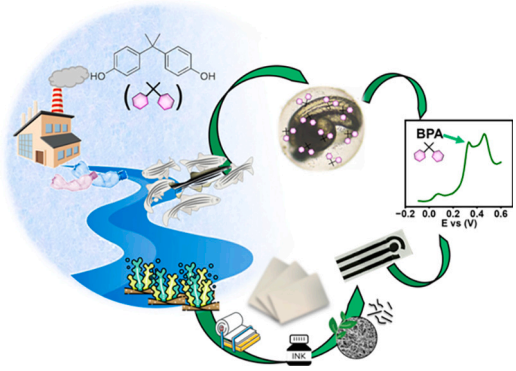

ARTICLE INFO

Keywords:
Paper-based device
In vivo studies
Nano-biochar
By-products
Zebrafish embryos
Lab-made sensors

ABSTRACT

Contaminant level assessment in in-vivo models and their environments remains an open issue that still needs smart solutions. Most of the analytical methods work as off-site analysis performed via instrumental techniques, while there is a lack of rapid strategies for real-time monitoring. Herein, self-contained Algae-paper sensors, produced using a sustainable approach, are proposed to determine Bisphenol A (BPA) bioconcentration in zebrafish embryos (*Z*-EBs) and to monitor the levels in culture medium.

Paper sensors were manufactured in series using a stencil printing approach and equipped with a by-product-derived nanomaterial (biochar) prepared in water via liquid-phase exfoliation, avoiding organic solvents. The best sensor paper-substrate and conductive-ink/biochar combination was studied. Algae paper, derived from seaweed biomass wastes, was able to support stencil printing and biochar with nano-fibrillar morphology, enabling the achievement of the required analytical performance.

* Corresponding authors.
E-mail addresses: fdellapelle@unite.it (F. Della Pelle), dcompagnone@unite.it (D. Compagnone).

https://doi.org/10.1016/j.scitotenv.2025.180529
Received 18 March 2025; Received in revised form 15 September 2025; Accepted 15 September 2025

Algae sensors' exploitability was demonstrated for *Z*-EBs exposed to different levels of BPA. The sensors accurately traced the BPA level variation in *Z*-EBs culture medium along the 96 h of the in vivo study (Relative Error − 14/+12 %) by simple immersion and measurement. Bioaccumulated BPA assessment in exposed Z-EBs was achieved via in-matrix calibration (Limit of Detection = 58 nM/13 μg L^{-1}), with reproducible data (RSD ≤ 8.8 %, $n = 3$) and quantitative recoveries (94–118 %), endorsing the sensor reliability. Algae sensors are useful in discriminating sublethal BPA levels characterized by different developmental delays of *Z*-EBs.

A sustainable sensor, produced following a circular economy route, was developed, demonstrating, for the first time, the exploitability of portable electrochemical devices for BPA determination for in vivo studies. The Algae-paper sensor allows both real-time monitoring of BPA levels during exposure studies and evaluation of bioaccumulation in *Z*-EBs at the end of the exposure period.

1. Introduction

Ecotoxicology is devoted to evaluating the impact of harmful agents on the ecosystem by studying their effects on living organisms (Ford et al., 2021); until now, these studies have been based mainly on the employment of vertebrate organisms. Nowadays, the increased bioethical sensitivity prompted the scientific community to explore invertebrates and lower vertebrates as in vivo equivalent models (Khabib et al., 2022; Pastorino et al., 2024). Among others, Zebrafish (*Danio rerio*), a lower vertebrate aquatic organism, attracted attention thanks to its high similarity with mammalians in terms of tissues and organogenesis, and high affinity with the human genome (Anita Rácz et al., 2021; Li et al., 2023). The zebrafish's small size, ease of reproduction, and brief life cycle result in facile handling and low-cost maintenance (Li et al., 2023); moreover, early-life stage zebrafish (embryonic stage) completely fulfill the requirements for 3Rs ethical principles (Anita Rácz et al., 2021). Therefore, Zebrafish is increasingly used in ecotoxicological studies for the evaluation of xenobiotics (Li et al., 2023), including bisphenol A (BPA) and its analogs (Gao et al., 2022; Kim et al., 2020; Mu et al., 2022; Vremere et al., 2022; Wu et al., 2017; Zhao et al., 2024).

BPA is a xenobiotic with estrogenic properties, classified as an endocrine-disrupting chemical (Rochester, 2013; Tarafdar et al., 2022). BPA is widely employed for the manufacturing of epoxy resin and polycarbonate that are used to produce 'food contact materials' (FCM), toys, appliances, and medical equipment (Ni et al., 2023); this massive use increases the chances of release in the environment, with contamination of aquatic and soil domains (Czarny-Krzymińska et al., 2023). BPA was classified as a Substance of Very High Concern (SVHC) under the Registration, Evaluation, Authorisation, and Restriction of Chemicals (REACH) regulation EC/1907/2006, Annex XIV, by the European Chemical Agency (European Comission, 2006). In this regard, the European Food Safety Authority has settled a tolerable daily intake of 0.2 ng per kg of body weight per day (ng/kg bW/day) (Lambré et al., 2023). Recently, BPA use was banned for the production of 'cups' and feeding bottles intended for infants and children (EU, 2018), and the EU Commission is considering extending the ban to all FCM (European Commission, 2024).

Ecotoxicological studies, regardless of the subject of the investigation, suffer from a lack of rapid and easy-to-use devices to determine and monitor the level of the tested 'toxic' during the exposure period, both in the model organisms and their cultivation environment; this deficiency results particularly relevant for bioconcentration/bioaccumulation studies (Gómez-Regalado et al., 2023). Indeed, the 'toxic' analyses are still mainly based on chromatographic techniques that require specific laboratory facilities, time-spending extraction/purification procedures, and trained personnel (Gómez-Regalado et al., 2023; Schäfer et al., 2015). The recent advancements in the electroanalytical field make electrochemical sensors a reliable solution for the determination of environmental contaminants (Liu et al., 2022); in particular, a plethora of electrochemical sensors were developed for the determination of BPA and analogues, proving high efficacy particularly in food and environmental matrices (Tajik et al., 2020; Zhang et al., 2021). Moreover, next-generation sensors are often characterized by smart and handheld layouts, designed to be usable even out of analytical chemistry laboratories (Silveri et al., 2025). Therefore, if properly conceived, electrochemical sensors may be employed as monitoring tools in ecotoxicological studies, streamlining the entire analytical process and enabling real-time and in situ detection of harmful agents; however, to the best of our knowledge, this approach has not been explored yet.

The current electro-analytical scenario reflects the trend promoted by the Sustainable Development Goals, where one of the main goals concerns improving sustainability and safeguarding the environment (Płotka-Wasylka et al., 2021; Sachs et al., 2019). In this framework, the concept of White Analytical Chemistry has gained importance, declining the 'analytical sustainability' beyond only greenness, including the evaluation of practical/economic facets and analytical 'figure of merits' (Nowak et al., 2021). Thus, the research for effective approaches to meet the WAC requirements remains a hot topic. In this context, the use of paper materials to fabricate sensors and devices represents a captivating opportunity, given the paper's ability to act as a functional substrate for conductive materials and for assembling multi-faceted paper-based devices and their active components (Arduini, 2022; Deroco et al., 2023). In this contest, chromatographic and office-grade papers are the most extensively employed for 'sensors development' purposes, while recycled and bioderived papers are little explored; the latter besides contributing to increasing sustainability, may potentially bring functional features and deserve to be better studied.

Different strategies have been introduced to make paper-sensor manufacturing more accessible/scalable and improve their performance. In this contest, recently stencil-printing has gained attention to obtain tailorable printed electronics (Sanchez-Duenas et al., 2023; Sfragano et al., 2020) since it requires readily available affordable materials and user-friendly machinery (Stefano et al., 2022). This printing approach relies on an adhesive stencil mask that can be effortlessly patterned with an office-grade cutting plotter, allowing boundless freedom for electrode design and in-series fabrication of multiple devices (Kay and Desmulliez, 2012; Kongkaew et al., 2022; Silveri et al., 2023a, 2023b). Nevertheless, stencil printing has mainly been employed using plastic/ceramic substrates, resulting in poorly explored for paper substrates (Fiori et al., 2025; Oliveira et al., 2023; Şen et al., 2024; Silva-Neto et al., 2023). On the other hand, despite the large use of nanomaterials to boost electro-analytical sensors (Caratelli et al., 2022), scarce use of biochar (BH) is reported for paper devices, despite its remarkable sustainability. BH is originated from the controlled pyrolysis of 'carbon reach biomasses', where organic matter is converted into 'more ordered' carbon nano/microstructures potentially useful from an electrochemical perspective (Amalina et al., 2022; Zheng et al., 2023). BH can be produced from industrial/agricultural by-products and wastes, giving them a second life in virtuous reuse circles. Thus, to improve the sustainability of paper devices, making them effective for real applications, the marriage between stencil-printing technology, 'emerging' sustainable papers, and nano-biochar produced from industrial wastes surely represents an interesting route that deserves exploration.

In this work, paper derived from seaweed biomasses (Algae paper) has been employed to build up stencil-printed nano-equipped

electrochemical sensors, according to circular economy and sustainable principles. The Algae sensors have been settled and optimized to determine Bisphenol A (BPA) bioaccumulated in zebrafish embryos (*Z*-EBs) and monitor the levels in culture medium. With this objective, the capability of Algae paper to act as functional support for stencil printing has been proven, comparing the performance with other office-grade and recycled papers, using PET as a control substrate. The combination of four conductive carbon-based inks with two different waste-derived biochars was tested on the whole set of substrates; the most performing combination resulted in Algae paper/carbon paste ink/nanofibrillar-biochar (Algae sensor). The Algae sensor was then challenged as a monitoring tool for studies conducted with Z-EBs exposed to different concentrations of BPA. Algae paper sensors demonstrated their ability to (i) monitor BPA directly in the Z-EBs culture medium in real-time and (ii) determine the bioaccumulated BPA in Z-EBs at the end of the exposure period, allowing the discrimination of sublethal BPA levels.

2. Materials and methods

2.1. Chemicals

Bisphenol A (BPA), potassium ferrocyanide, potassium ferricyanide, potassium chloride, sodium phosphate dibasic dihydrate, sodium cholate, calcium chloride dihydrate, magnesium sulfate heptahydrate, sodium bicarbonate, dimethyl sulfoxide (DMSO) and methanol were purchased from Sigma Aldrich (St Louis MO, USA). All the experiments were carried out using Milli-Q grade water 18.2 MΩ cm^{-1} (Millipore, Bedford, MA, USA).

2.2. Apparatus

The design of the sensors was patterned using Adobe Illustrator 2024 software. A Cameo 4 cruft-cutter plotter (Silhouette America®, Lindon, USA) governed by Silhouette Studio 4.4 software was used to tailor the stencil masks. Electrochemical experiments were performed using a Palmsens 4 potentiostat/galvanostat/impedance analyzer (Palm Instruments BV, Houten, Netherlands) managed by PS trace software. A probe sonifier SFX550 (Sonifier® SFX series; Branson Sonic Power Co., Banbury, Connecticut, USA) furnished with 1/8″ tapered Microtip (wattage Output: 550 W; frequency Output: 20 kHz) was used for the sonochemical water-phase exfoliation/nanodispersion of BHs. A GeminiSEM 500 (Zeiss Co., Oberkrochen, Germany) equipped with an InLens detector for micrograph acquisition was used for field emission scanning electronic microscopy (SEM), using an acceleration potential of 3 kV and a working distance of 3 mm.

2.3. Sensor substrates and conductive inks

Algae paper was purchased from LifeMaterials (Montelupo Fiorentino, Toscana, Italy) (weights 120 g cm^{-2}), *Kraft* paper from Eles Vida company (120 g cm^{-2}) was purchased from an online supplier, Navigator paper (*Navi*) was purchased from Navigator company (Setubal, Portugal) (120 g cm^{-2}), Risma-Luce paper (*Luce*) was purchased from Favini company (Rossano Veneto, Veneto, Italy) (120 g cm^{-2}). Polyethylene terephthalate sheets (*PET*; 0.18 mm) were purchased from Fellowes (Itasca, Illinois, USA). Self-adhesive vinyl stencil masks were purchased from TINYYO (Parson drove, Wisbech, UK).

Conductive inks: 'carbon paste' (i-CP) and 'carbon sensor paste' (i-CSP) were purchased from Sun Chemical (Parsippany-Troy Hills, New Jersey, USA), 'carbon/graphite for screen-printing paste' (i-GSPP) and 'graphite ink for flexographic printing' (i-GFP) were purchased from Sigma Aldrich (St Louis MO, USA). Nail polish for paper-based sensor insulation was purchased from a local market.

2.4. Biochar production and suspension in water

Nanofibrillar biochar (BH-F) was developed and formulated by 'theLAB' - Materials, Design and Products (San Ginesio, Italy), and produced and supplied by FreyZein GmbH (Dornbirn, Austria). Briefly, black liquor, a eucalyptus-derived woody biomass was obtained from the kraft process (Bukhari et al., 2021). This mass rich in lignin was subjected to a drying treatment (40 °C, 12 h), and subsequently grounded in a planetary ball miller for 2 h at 250 rpm (40 mm diameter balls). Afterward, a preliminary thermal treatment was carried out at 250 °C at atmospheric pressure, and then a carbonization process was performed at 1200 °C for 8 h under saturated atmosphere. Finally, a further ball milling process was performed for 24 h at 300 rpm, (balls with 10 mm diameter). Amorphous biochar (BH-A) was obtained using pellets of walnut shells as feedstock. In brief, the pellets underwent a pyrolytic micro-gasification process at 500 °C in a Pyreg reactor (GmbH, Dörth, Germany) in CO_2 sequestering conditions. Then, the obtained biochar powder was manually grounded to reduce the particle size.

The nanobiochars suspension was obtained via a liquid phase exfoliation-like process in water (Bukhari et al., 2021). Firstly, 5 mg of BH powder were placed in a 5 mL water solution containing sodium cholate at 1 mg mL^{-1}. Then, after a brief 'homogenization' in bath sonicator (5 min), the suspension was sonicated with the high-power probe sonicator SFX550 equipped with a microtip (details in Section 2.2) employing a pulsed program (2 s ON, 1 s OFF) for a total treatment time of 1 h and 2 h for BH-F and BH-A, respectively. During the sonochemical treatment, the 'sample' was placed in an ice bath to keep the temperature under control, setting the alarm temperature at 10 °C. Afterward, the BH dispersion was centrifugated at 20000 g for 15 min in 5 mL Eppendorf Tubes, discarding the supernatant containing the sodium cholate excess; the pellet was resuspended in 5 mL of Milli-Q grade water, and used for paper sensor modification (details in Section 2.5).

2.5. Algae paper sensors in-series manufacturing

Scheme 1 graphically sketches the main steps of paper sensor manufacturing. Initially, the cruft-cutter plotter patterned stencil mask was adhered onto the Algae paper sheet, then 1 g of i-CP ink was spread using a squeegee, ensuring the uniform formation of working (WE), counter (RE), and pseudo-reference (pRE) electrodes with the respective contacts. Later, the mask was removed, and a curing at 60 °C for 30 min carried out. Afterward, the contacts were insulated by spreading nail polish on each side of the sensors, drying at room temperature. Eventually, the working electrode surface (3 mm Ø) was modified via drop-casting, using 6 μL of the BH-F suspensions at the concentration of 1 mg mL^{-1} (biochar details in Section 2.4).

The same procedure was followed to fabricate the sensors on the other paper substrates (kraft, Navi, and Luce), testing also the other inks (i-CSP, i-GSPP, and i-GFP ink) and biochar (BH-A); for i-GFP ink 10 min curing was performed in agreement with the manufacturer's recommendations. The PET-based sensors were manufactured using the same procedure; in this case, the sensor contacts insulation was carried out with a complementary sheet of polyethylene terephthalate-ethylene vinyl acetate (PET-EVA; 0.10 mm, purchased from Fellowes, Itasca, Illinois, USA) using a thermal roll laminator (Pavo 8,038,718 from Unbekannt, Germany).

2.6. Electrochemical and electroanalytical characterization

The electrochemical features of the whole set of stencil-printed paper sensors were investigated employing an external counter electrode (CE) and reference electrode (RE), using a Pt wire and Ag/AgCl (3 M KCl), respectively.

The sensors' electrochemistry was explored via cyclic voltammetry (CV) at 25 mV s^{-1} using 5 mM $[Fe(CN)_6]^{3-/4-}$ in 0.1 M KCl as redox probe. The BPA electochemistry at the paper-sensors was investigated in

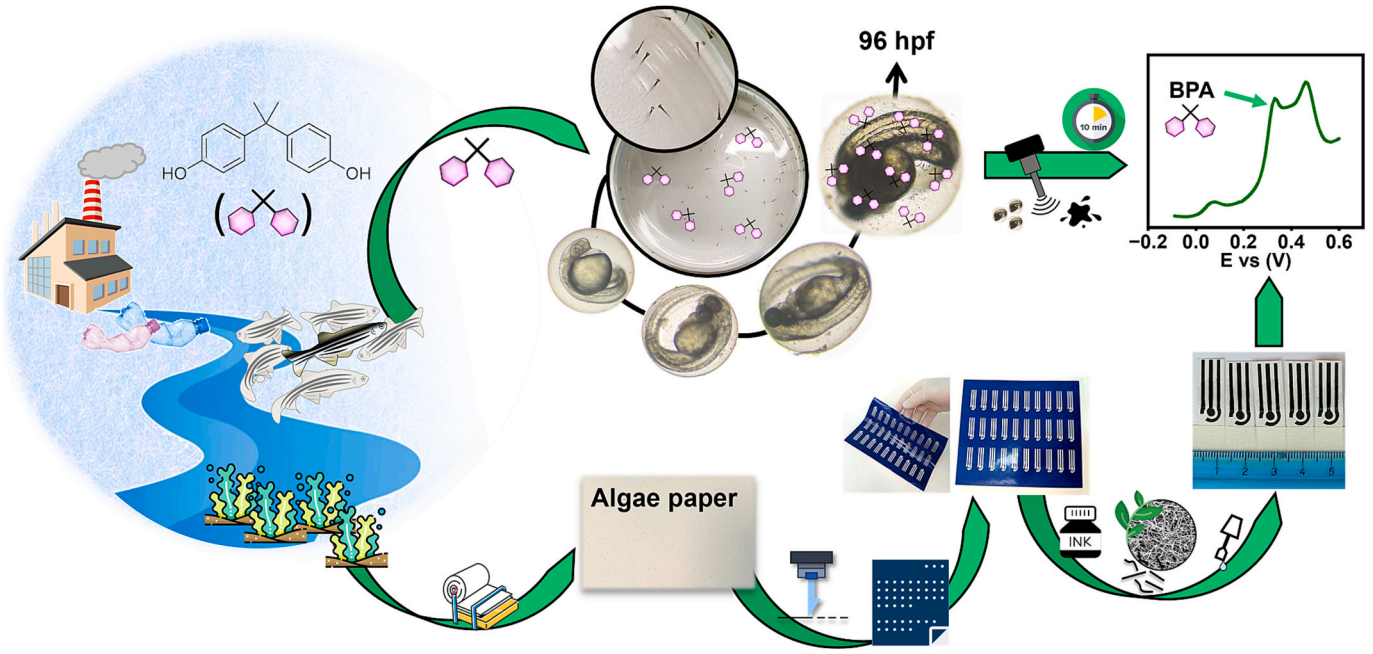

Scheme 1. Graphical sketch of the work concept and circularity, enclosing the graphic summary of the Algae paper sensor production and the application in zebrafish embryos exposure studies.

0.1 M phosphate buffer pH = 7 (PB) performing CV at 25 mV s^{-1} and differential pulsed voltammetry (DPV) using a 25 ms pulse width, 75 mV as modulation amplitude and a scan rate of 25 mV s^{-1}.

A deeper investigation of the electrochemical properties of Algae paper sensors was performed using 5 mM of $[Fe(CN)_6]^{3-/4-}$ in 0.1 M KCl as redox probe, performing CVs at increasing scan rate, and using electrochemical impedance spectroscopy (EIS) to extrapolate the charge-transfer resistance (R_{CT}). EIS was carried out by scanning the frequencies between 10^5 and 10^{-1} Hz, using a sinusoidal wave of 5 mV amplitude, setting the potential at open circuit. Double layer capacitance (C_S) investigation was performed via CV at increasing scan rates in 0.1 M KOH, working in the non-faradic potential window.

2.7. Zebrafish embryos exposure studies

Animal experiments were performed in agreement with Directive 2010/63/EU of the European Parliament and the Council (September 22, 2010) concerning the protection of animals used for scientific purposes. Adult zebrafish (wild-type AB strain) were housed at the University of Teramo (breeding code 041TE294) in 3.5 L ZebTec tanks (Tecniplast SpA, Buguggiate, Italy) within a recirculating aquatic system. The water temperature was maintained at 28 °C, with a pH of 7.0 ± 0.2, conductivity at 500 ± 100 μS cm^{-1}, and dissolved oxygen levels of 6.1 mg L^{-1}. The photoperiod was set to 14 h of light and 10 h of darkness. Chemical parameters: 02 mg L^{-1} ammonia, 0.02 mg L^{-1} nitrite, and 21.3 mg L^{-1} nitrate. Zebrafish were fed live *Artemia salina* twice daily, with additional ZEBRAFEED 400–600 dry feed (Sparos, Olhão, Portugal). In the afternoon before spawning, ten pairs of zebrafish (1:1 female-to-male ratio) were transferred to 1.7 L breeding tanks (beach-style design; Tecniplast SpA, Buguggiate, Italy). The following day, immediately after spawning, fertilized eggs were collected using a sieve, thoroughly rinsed with deionized and distilled water, and divided into groups of about 100 eggs. The eggs were then placed in Petri dishes and incubated at 27 °C.

Zebrafish embryos (*Z*-EBs) were inspected under a dissecting microscope and selected for further experiments upon reaching the blastula stage, according to Kimmel et al. (Kimmel et al., 1995). Approximately 100 embryos (4–16 cell stage) were transferred to crystallizing dishes (115 mm in diameter, 1000 mL capacity) containing 200 mL of the 'culture medium'. The culture medium was tested at different sublethal BPA concentrations (0.5, 1, 2, 4, and 8 mg L^{-1}; corresponding to 2.19, 4.38, 8.76, 17.52, 35.04 μM), according to our previous *Z*-EBs toxicological studies (Vremere et al., 2022).

Z-EBs were exposed to BPA for 96 h post-fertilization (hpf) at 26 ± 1 °C under a 14-h light/10-h dark cycle. A dual approach was used for BPA exposure, combining static conditions (without renewal of the exposure solution) and semi-static conditions (renewing the exposure solution every 24 h). A negative control group was maintained in 'reconstituted water' prepared according to Organisation for Economic Co-operation and Development test guidelines 203 (OECD TG203) (OECD, 2019), and the 'solvent control' group was exposed to 0.1 % DMSO.

2.8. BPA determination via algae paper sensors in exposure studies

The BPA analysis in *Z*-EBs model was performed via DPV (parameters in Section 2.4), using complete self-contained Algae paper sensors (Scheme 1); the latter consisted of CE and pseudo-RE, both made of graphitic ink, integrated with the WE (manufacturing detailed in Section 2.5).

2.8.1. BPA monitoring in zebrafish embryos culture medium

'Fresh' and 'exhausted' *Z*-EBs culture medium, understood as the medium at the beginning and the end of the exposure studies without BPA, were taken as 'blank matrixes' and used to build up in-matrix calibrations. To this aim, culture media were diluted 25:75 (*v*/v) in PB and spiked with increasing concentrations of BPA (0.25–6 μM), then DPV measurements were performed using the Algae paper sensor.

The determination of BPA in Z-EBs culture media during exposure studies was performed at different times, diluting the 'sample' 25:75 (v/v) in PB, and running the DPV measure with the Algae paper sensor.

2.8.2. Determination of BPA in zebrafish embryos

Zebrafish embryos not exposed to BPA were taken as blank matrix and used to build up in-matrix calibration. Briefly, 0.1 g of Z-EBs at 96 hpf were collected and placed in 5 mL of methanol and were sonicated

for 10 min (30 % amplitude, continuous mode; SFX550 sonifier details in Section 2.2) maintaining the temperature below 10 °C.

'Homogenized Z-EBs' were then centrifugated at 10000 g for 10 min and the supernatant recovered. Eventually, the extraction solvent was removed employing a SpeedVac Vacuum Concentrator (Thermo Fischer, Waltham, Massachusetts, USA), and the pellet was resuspended in 0.2 mL of methanol. The obtained 'blank matrix' was diluted with a dilution ratio of 15:85 (v/v) in PB, and then spiked with increasing concentration of BPA (0.25–6 μM) to build-up the in-matrix calibration, performing DPV measures with the Algae paper sensor.

The same protocol was applied for the BPA-exposed Z-EBs (96 hpf); then, the samples were analyzed through DPV with the Algae sensor (Z-EBs BPA exposure detailed in Section 2.7), and data extrapolated using the in-matrix calibration.

3. Results and discussion

The idea beyond this work was to develop paper sensors to effectively determine and monitor BPA in Zebrafish-based exposure studies. Paper derived from seaweed biomass (Algae paper) demonstrated superior behavior, and an affordable sensors manufacturing technique (stencil-printing) along with nanomaterial from the by-product biochar (BHs), allowed to ensured the required performance. Scheme 1 resumes the circularity of the proposed approach, where biomass coming from an aquatic ecosystem (Algae paper), allowed integrated sensor smart construction for the determination of the ubiquitous water ecosystem contaminant BPA.

3.1. Paper sensors manufacturing and components selection

This section reports the studies concerning the selection of the sensor substrates and conductive ink; both components were optimized in combination with two kinds of water-dispersed nanostructured biochars, characterized by nanofibrillar (BH-F) and amorphous (BH-A) structures. The sensors in series manufacturing strategy is graphically resumed in Scheme 1 and detailed in Section 2.5.

3.1.1. Substrate selection

The sensor support type in the stencil printing process was studied using carbon paste ink (i-CP) in combination with BH-A and BH-*F. algae* paper from seaweed biomass (Algae paper), paper produced through kraft process (Kraft), and office-grade papers (Luce and Navi) were evaluated, together with polyethylene terephthalate (PET), a polymeric substrate commonly used for printed sensors fabrication; details of the employed substrates are reported in Section 2.3.

Fig. S1A-B reports the peak intensity (i_{pa}) and the peak-to-peak separation (ΔE) extrapolated from cyclic voltammetry (CV) performed with the redox probe $[Fe(CN)_6]^{3-/4-}$; the relative cyclic voltammograms are displayed in Fig. S2. For all the substrates the modification with both kinds of BHs induced an i_{pa} increase and ΔE decrease, indicating an overall improvement of the electron-transfer ability and electroactive area (Bukhari et al., 2021; Cancelliere et al., 2019, 2023). Similar performances were obtained for BH-F and BH-A on PET.

The BPA electrochemistry was studied via cyclic voltammetry (CV) for the whole set of stencil-printed sensors; the obtained plots are reported in Fig. S3. All sensors showed a CV profile characterized by a sharp and irreversible anodic faradic peak at $+0.583 \pm 0.007$ V (vs Ag/AgCl), which is attributed to the oxidation of the hydroxylic groups of the phenolic rings to the corresponding quinones through an irreversible $2e^-/2H^+$ reaction (Zhang et al., 2021). BH-F induces a higher boost of BPA electrooxidation compared to BH-A. Interestingly, Algae and Kraft papers, resulted in the more active, followed by PET, whereas lower responses were observed for Luce and Navi papers.

BPA was analyzed via differential pulsed voltammetry (DPV) to better discern the sensors' electro-analytical potential. Fig. S1C shows the faradic peak intensity current obtained for 5 μM BPA, whereas the relative voltammograms are depicted in Fig. 1.

The outcomes emphasize the previous observation, where BH-F returned significantly higher performance, whereas only a slight improvement was obtained using BH-A. These results suggest that, despite similar crude electron-transfer features (see Fig. S1), BH-F possesses higher sensing ability toward BPA, confirming the biochar 'electroactivity' for phenolic compounds already reported in the literature (Bukhari et al., 2021).

More interestingly, among the tested substrates the DPV analysis indicates Algae paper equipped with BH-F as the most performing sensor, followed by Kraft ~ PET, Navi, and Luce paper. From the voltammograms, it is evident the influence of the paper substrate; this gave rise to additional unknown peaks particularly evident for Kraft, Luce, and Navi papers. To shed light on the nature of the additional peaks observed, Fig. 1F reports the DPV scans performed in only phosphate buffer (0.1 M pH = 7; PB) at the different bare sensors. Each substate possesses a diverse inherent electrochemistry in the potential window analyzed. Luce and Navi's papers exhibit an additional sharp peak at ~0.75 V (vs Ag/AgCl), whereas Kraft's paper is characterized by the presence of a prominent peak at ~0.4 V (vs Ag/AgCl). These 'peaks' are likely due to the paper's 'chemical composition', and probably contribute to make the BPA signal less intense/resolved. On the other hand, the Algae paper sensor returns a 'clean' voltammetric profile, similar to PET.

The obtained results prove for the first time the exploitability of Algae paper for electrochemical analysis and the ability to support the stencil printing process. Although comparable electron-transfer abilities were observed for the different substrates, Algae paper returned superior performance for BPA electrooxidation. This feature can be attributed to the nature of the seaweed biomass used for Algae paper manufacturing, quite different from tree-based paper. In Algae paper, lignin is either absent or present in low amount, while it is naturally abundant in wood pulp, and thus it may be present in the derived office/kraft paper. Moreover, it is reported that cellulose derived from Algae has a much larger surface area compared to plant-derived cellulose (Baghel et al., 2021). It is then reasonable to hypothesize that, thanks to the peculiar structure, the Algae paper cellulosic matrix worked as an effective scaffold to entrap the carbon ink, leading to the formation of a conductive surface suitable for accommodating the nanofibrillar network of BH-F, allowing to unleash its full electrocatalytic potential. In addition, the inert electrochemistry shown by the Algae paper substrate helped to increase the signal-to-noise ratio, conferring remarkable advantages with respect to the other cellulosic substrates. Thus, Algae paper was selected as a substrate for conductive ink selection.

3.1.2. Conductive ink selection

Carbon paste inks usually employed for screen-printing, namely 'carbon paste ink' (i-CP) and 'carbon sensor paste' (i-CSP), together with 'graphite for screen-printing paste' (i-GSPP), and 'graphite ink for flexographic printing' (i-GFP) were tested with algae paper.

To understand the printed inks' electrochemistry $[Fe(CN)_6]^{3-/4-}$ was employed as redox probe. Fig. 2A-D report the different outcomes of the inks on Algae paper.

i-CP (A) and i-CSP (B) inks return a similar trend, where both BHs improve the electrochemical performance with high faradic peaks and low ΔEs. On the other hand, remarkable differences were observed for i-GSPP (C) and i-GFP (D) ink responses. In particular, for the i-GSPP the modification with both BHs induced only a slight rise of the faradic peaks current, with no effect on ΔE. Thus, this ink only slightly widens the electro-active area. The i-GFP ink showed only tiny faradic currents, with no improvement after modification with BH. The latter behavior could be ascribed to the i-GFP morpho-chemical structure characterized by a surface 'patina', not favorable to electron-transfer processes as already reported (Silveri et al., 2024).

The electrosensing ability toward BPA of the sensors was also tested via CV (Fig. 2E-H) and DPV (Fig. 2E-H insets and Fig. S4). The data

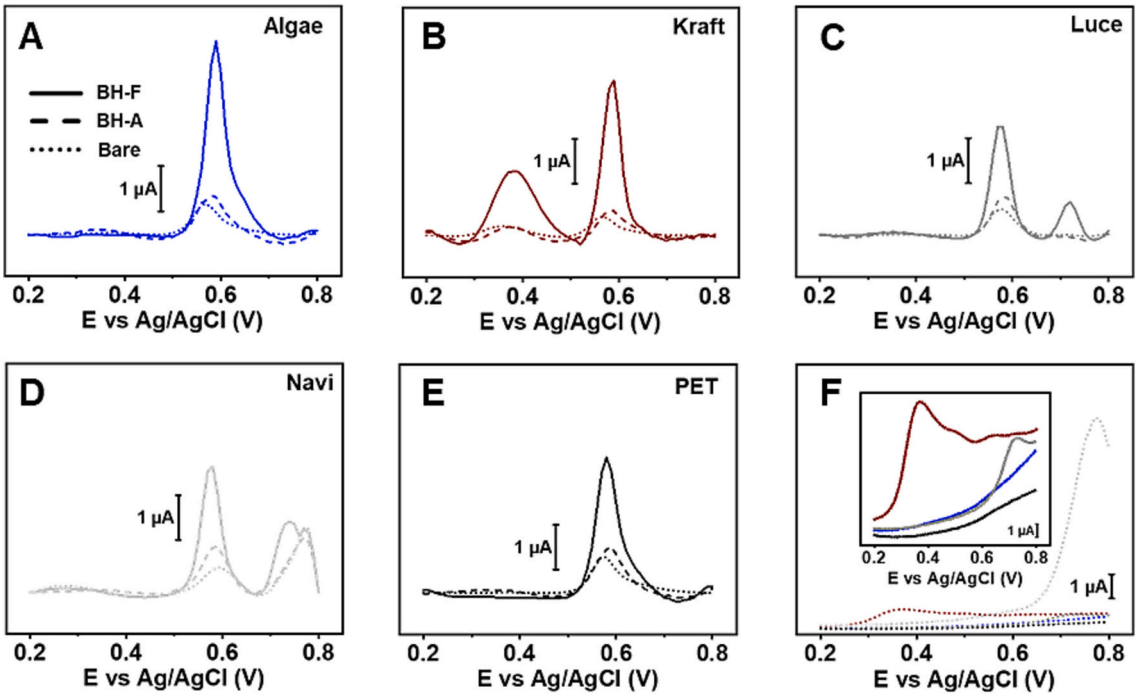

Fig. 1. Differential pulsed voltammograms of 5 μM BPA in PB at stencil-printed sensors realized onto different substrates. (A) Algae paper, (B) Kraft paper, (C) Luce paper, (D) Navi paper, and (E) PET. Legend: full lines = BH-F, dashed lines = BH-A, dotted lines = bare sensor. (F) Raw differential pulsed voltammograms in PB only (blank measures) at the different bare sensors; the inset is the same figure without the Navi paper sensor.

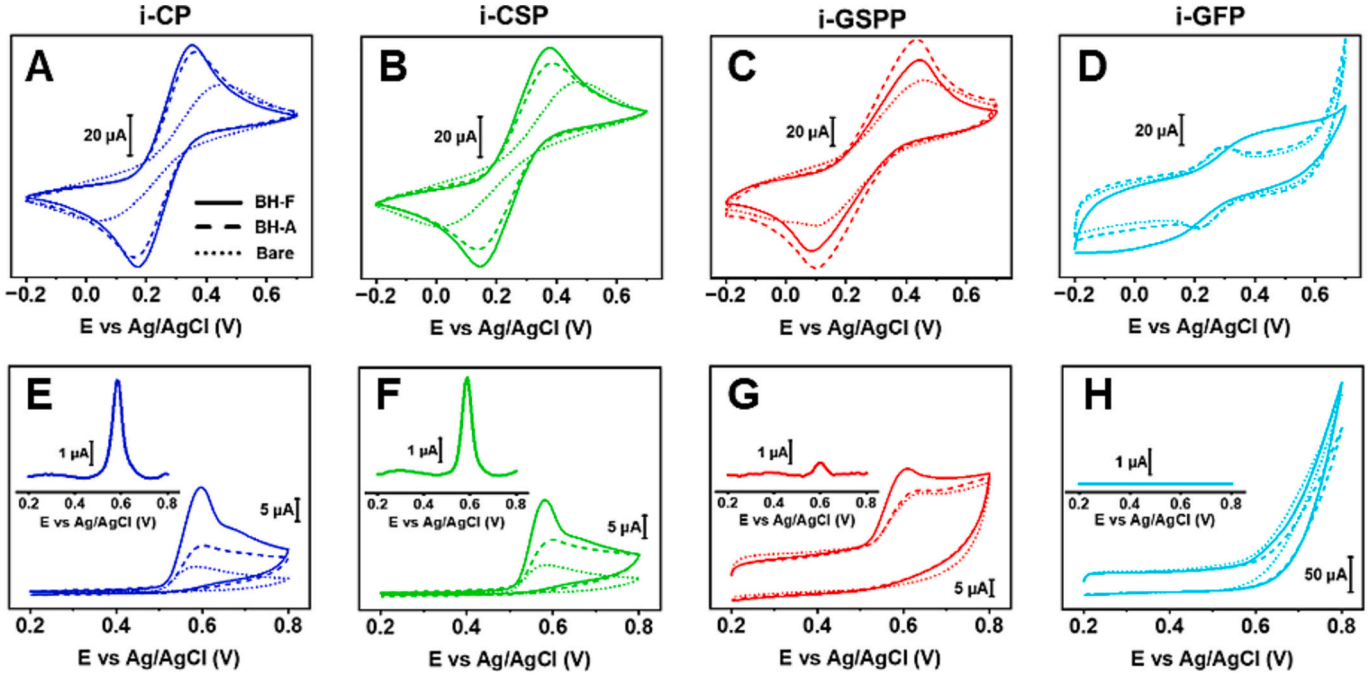

Fig. 2. Electrochemical output of stencil-printed sensors realized on Algae paper using different conductive inks. Cyclic voltammograms of 5 mM $[Fe(CN)_6]^{3-/4-}$ in 0.1 M KCl for (A) i-CP, (B) i-CSP, (C) i-GSPP, (D) i-GFP inks. Cyclic voltammograms of 250 μM BPA for (E) i-CP, (F) i-CSP, (G) i-GSPP, (H) i-GFP inks; the insets report differential pulsed voltammograms of 5 μM BPA obtained at the respective BH-F modified sensor. Legend: full lines = BH-F, dashed lines = BH-A, dotted lines = bare sensor. CV performed at 25 mv s^{-1}.

proved the superior performance for the combination i-CP/BH-F (E), followed by the i-CSP/BH-F (F). i-GSPP in the presence of BH-F (F) evidences only slight improvements of the bare ink, while no significant changes were recorded in presence of BH-A; the CV signals allow to attribute these scarce performances to the huge capacitive currents, that result in a signal-to-noise ratio (S/N) ~20 folds lower compared to the other inks ($S/N_{i\text{-}CSPP} = 1.9$; $S/N_{i\text{-}CSP} = 38.1$; $S/N_{i\text{-}CP} = 47.2$); the S/N was extrapolated from the ratio between the faradic peak of BPA electrooxidation and the capacitive current. i-GFP (H), pristine and BH-modified, gave no response in the presence of BPA, confirming the

poor electroactivity.

Summing up, Algae paper can support stencil-printing performed with different conductive inks, leading to the formation of transducers with diverse features. Among the others, i-CP and i-CSP are the most appropriate to express the superior electrocatalytic features toward BPA driven by the BHs modification. These outcomes could be ascribed to the superior electron-transfer abilities obtained after the BHs modification (proven by the lower ΔE values), which goes beyond a mere increase of the electro-active area (i-CSPP), while i-GFP showed no improvement at all. Moreover, as previously discussed, the BPA electro-sensing is likely affected by the capacitive current, as confirmed by the highest S/N obtained from i-CP and i-CSP. In light of this, i-CP was selected among the inks and employed for following studies.

3.2. Algae paper sensors characterization

Algae paper sensors obtained using i-CP with both BHs were deeply characterized to shed light on the electrochemical and morphological features. Charge-transfer resistance (R_{CT}) was explored via electrochemical impedance spectroscopy (EIS). Fig. 3A depicts the Nyquist plots obtained for the bare and BH-modified Algae sensors, the relative charge-transfer resistance (R_{CT}) values extrapolated fitting the data with the Randles-equivalent circuit are reported in Fig. 3C (light green bars).

i-CP on Algae paper (bare sensor) is characterized by a wide semicircle characterized by the highest R_{CT} value (4035.5 ± 639.5 Ω), while the BH presence drives a substantial reduction of the semicircle. The decrease in the R_{CT} appears more pronounced for BH-F modification (181.3 ± 1.1 Ω) than BH-A (568.7 ± 43.5 Ω).

The 'electron-transfer features' for Algae paper sensors were evaluated, performing CVs at increasing scan rates in $[Fe(CN)_6]^{3-/4-}$; the relative voltammograms are displayed in Fig. S5A—C. A linear relationship between the faradic intensity current and the square root of the scan rate (Fig. S5D) was achieved, indicating a diffusion-limited reaction for the probe (Blandón-Naranjo et al., 2018), and the obtained data were used to estimate the electro-active surface area (ECSA) according to Randles-Sevick method (Bard and Faulkner, 2001). Similar ECSA were obtained for Algae paper enclosing BH-A (9.85 ± 0.17 mm^2) and BH-F (11.04 ± 0.21 mm^2), resulting ~2 folds larger than the bare ink (5.49 ± 0.34 mm^2). The same trend was obtained for the heterogeneous electron transfer constant (k^0), where the two BHs display k^0 ~ 2 folds higher (BH-A: 2.50 × 10^{-3} ± 0.01 × 10^{-5} cm s^{-1}; BH-F 2.45 × 10^{-3} ± 5.00 × 10^{-5} cm s^{-1}) than the pristine ink (1.35 × 10^{-3} ± 5.00 × 10^{-5} cm s^{-1}); k^0 was extrapolated according to Nicholson's theory for quasi-reversible systems (Della Pelle et al., 2020; Nicholson, 1965).

Double-layer capacitance (C_s) was also studied since is well-established that in electrochemical sensors based on nanomaterials, excessive capacitive currents negatively affect the S/N ratio (Hernández-Rodríguez et al., 2020). C_s was studied via cyclic voltammetry in 1 M KOH under increasing scan rates, recording the current in the non-faradaic region. Fig. 3B reports the linear relationship between the non-faradic density current (j, μA cm^{-2}) and the scan rate (ν, V s^{-1}), described by the equation $j = C_s\nu$; C_s values extrapolated from the slope of the latter eq. [54] are reported in Fig. 3C (cyan bars), while Fig. S5E depicts CV achieved at 100 mV s^{-1} for all sensors. Interestingly, BH-A led to a significantly larger C_s (3926 ± 237 μF cm^{-2}) compared to BH-F (2246 ± 138 μF cm^{-2}). This explains the worse performance of BH-A compared with BH-F for the BPA electrosensing observed in Section 3.1, where the higher intrinsic 'capacitive current' of BH-A hinders the faradic signal of the BPA in electrooxidation.

Eventually, morphological and elemental characterization was performed via scanning electronic microscopy (SEM) and energy-dispersive X-ray spectroscopy (EDX). Fig. 3D-E reports the pristine Algae paper and Algae paper with i-CP ink. Algae paper substrate (D) is characterized by a fibrillar structure, typical of cellulosic-based materials (Vicente et al., 2017), after i-CP printing (E), it disappears and is replaced by a uniform and crack-free film dominated by graphitic flakes. Fig. S6 EDX spectra highlight a remarkable elemental change, where Algae paper is characterized by a C/O ~ 1.3, that after i-CP printing becomes 10-fold higher ($C/O_{i\text{-}CP}$ ~ 13); moreover, the trace of additional elements (Ca, Mg, and Al), naturally present in Algae biomasses (Olsson et al., 2020; Tonon et al., 2022) after the printing disappears, confirming an effective covering of the paper substrate. Different surface morphologies were

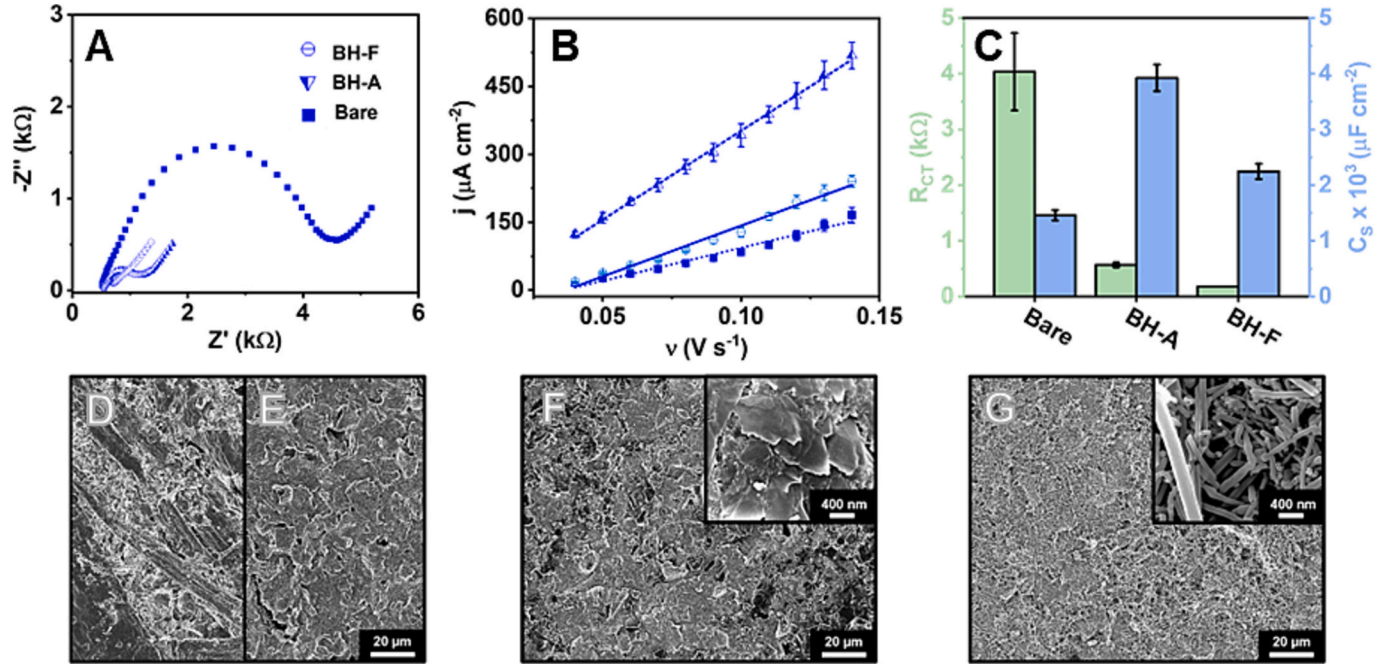

Fig. 3. Electrochemical and morphological characterizations of i-CP Algae paper sensors. (A) Nyquist plot obtained in 5 mM $[Fe(CN)_6]^{3-/4-}$ in 0.1 M KCl and (B) Linear relationships between non-faradic density current and scan rate obtained in 1 M KOH. Legend: BH-A (triangle dots), BH-F (round dots), bare sensor (square dots). (C) Charge transfer resistance (R_{CT}) and double layer capacitance (C_S) values. SEM micrographs of (D) Algae paper substrate, (E) algae paper sensor with i-CP only, (F) algae paper sensor with i-CP/BH-A, (G) algae paper sensor with i-CP/BH-F. Signal acquisition InLens Mag 500 x. Insets signal acquisition InLens Mag 30 Kx.

observed after BH-A (Fig. 3F) and BH-F (Fig. 3G) modification. In both cases, the surface of the ink results uniformly covered by nanometric amorphous flakes (BH-A) and nanofibers (BH-F); the magnification reported in the insets allows to state that in the film both BH preserve the nanometric domain (Bukhari et al., 2021; Cancelliere et al., 2019, 2023). These observations prove the Algae paper/i-CP ability to accommodate uniformly nanostructured materials with different morphologies. EDX analysis pointed out a similar C/O decrease (C/O ~ 9) for both BH (Fig. S5), due to a higher amount of oxygenated moieties compared to the pristine ink (Bukhari et al., 2021).

3.3. BPA determination in culture medium and zebrafish embryos

This study was conducted using the Algae sensor (i-CP/BH-F), composed of integrated working (WE), counter (CE), and pseudo-reference (pRE) electrodes, to have a fully integrated and handheld device. Algae paper sensor manufacturing is sketched in Scheme 1 and detailed in Section 2.5.

The complete sensor reliability was proved by comparison to the sensor using external CE (Pt wire) and RE (Ag/AgCl; 3 M KCl) electrodes for the BPA response using DPV, in agreement with Banks et al. (Sigley et al., 2023). Fig. S7 proves that the integrated pRE, made of i-CP ink, as expected, induces an electrooxidation overpotential shift toward lower potentials. Nevertheless, this potential resulted stable and reproducible (BPA E_{ox} = 248.5 ± 7.2 mV; RSD = 2.9 %, n = 3), with faradic peak currents comparable with external RE (i_{pa}-RE/ i_{pa}-pRE = ~1), endorsing the reliability of the proposed integrated Algae paper sensor for BPA electrosensing.

Algae paper-based sensor was thus challenged to monitor BPA in *Z*-EBs culture medium along exposure studies. To this aim, dose-response curves of BPA in the range between 0.25 and 6 μM (corresponding to 0.06 and 1.37 mg L^{-1}) were built up in 'fresh' and 'exhausted' *Z*-EBs culture medium, taken at the beginning and the end of the exposure study.

As control, the calibration was conducted also in phosphate buffer (0.1 M, pH = 7; PB). Fig. 4A-B returns the differential pulsed voltammograms obtained in PB (A), fresh (B), and exhausted (C) culture medium, whereas the relative calibration curves are depicted in Fig. 4F (blue, light blue, olive green curves).

The calibration curves were similar, with practically identical figures of merit (see Table S1). Thus, taking into consideration the calibration obtained in PB for simplicity, Algae paper allows to obtain a sensitivity of 11.99 ± 0.40 μA cm^{-2} μM and a nanomolar LOD (48 nM / 11 μg L^{-1}); the LOD was estimated through the formula LOD = [(3 x σ)/m], where σ is the standard deviation of the intercept and m is the value of the slope. The sensor returned remarkable inter-device reproducibility in all the analysis media (RSD ≤ 4.7 %; n = 3); the latter was estimated considering the slope of each calibration curve performed in triplicate (PB = 0.847 ± 0.029 μA $μM^{-1}$; fresh medium = 0.808 ± 0.038 μA $μM^{-1}$; exhausted medium 0.831 ± 0.024 μA $μM^{-1}$). The obtained data prove the absence of a matrix effect for fresh and exhaust culture medium, further confirmed by the absence of peaks in the 'blank measurement' carried out in the 'BPA-free' medium (Fig. 4A-C, dashed curves). The accuracy of the BPA determination was also demonstrated via recovery studies performed in fresh and exhausted culture media, at BPA levels used for the *Z*-EBs exposure studies (i.e. 0.5, 1, 2, 4, and 8 mg L^{-1}; detail reported in Section 2.7). In both media satisfactory recoveries were obtained (94.8–108.1 %), together with acceptable reproducibility (RSD ≤ 9.2 %, n = 3).

The Algae paper sensor's capability to detect BPA in zebrafish embryos was then tested. Z-EBs 'blank-matrix' was obtained according to Section 2.7 and fortified with BPA levels between 0.25 and 6 μM. Fig. 4D reports raw DPV plots obtained for the *Z*-EBs blank matrix (dashed curve) and after BPA-fortification (full curve). The blank Z-EBs show two unknown peaks at ~ +0.1 V and ~ +0.5 V (vs pRE), which can be attributed to electro-active species released from the zebrafish embryo lysate. Nevertheless, the Algae sensor allows BPA electrooxidation also in this complex matrix, giving rise to a sharp and distinguishable anodic

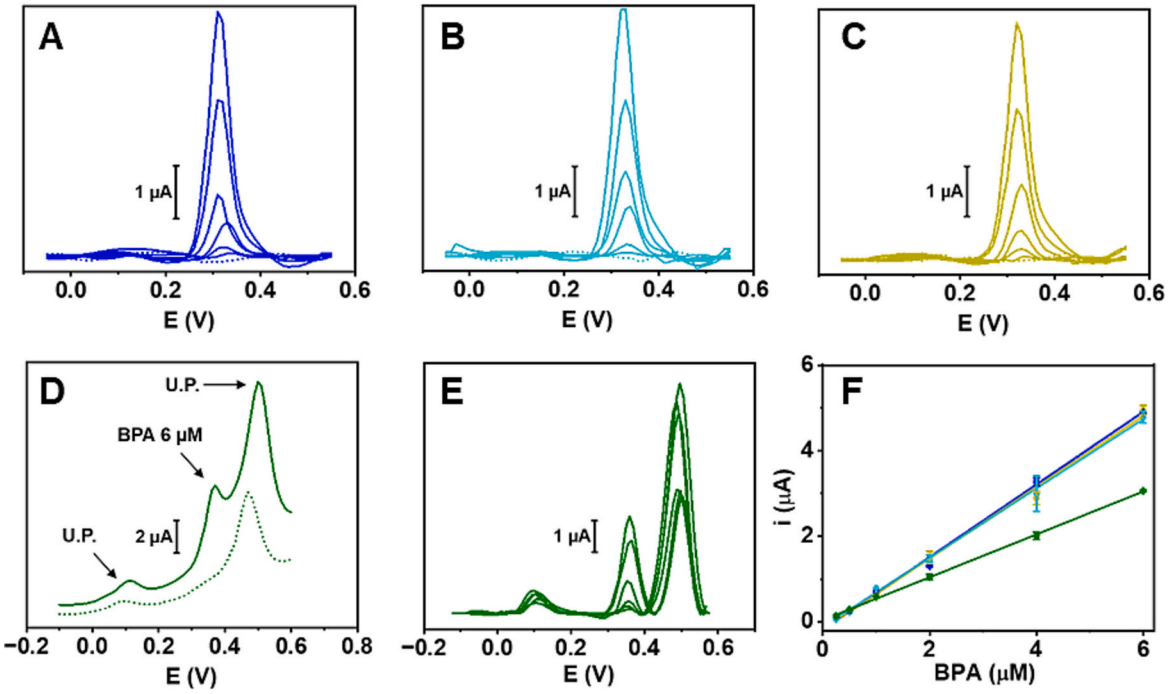

Fig. 4. Differential pulsed voltammograms for increasing BPA concentrations (from 0.25 to 6 μM) obtained in (A) PB only, (B) fresh *Z*-EBs culture medium, and (C) exhausted Z-EBs culture medium. The voltammograms depict the signal after the baseline correction. (D) Raw differential pulsed voltammograms of unfortified (dotted curve) and BPA-fortified (full curve) Z-EBs matrix. (E) Differential pulsed voltammograms obtained in Z-EB matrix fortified with increasing BPA concentrations (from 0.25 to 6 μM); U.P. = unknown peak. The voltammogram depicts the signal after the baseline correction. (F) Dose-response curves obtained in PB only (blue curve), fresh Z-EBs culture medium (light blue curve), exhausted *Z*-EBs culture medium (olive green curve), and Z-EBs matrix (green curve).

peak at 0.360 ± 0.005 V (vs pRE). Fig. 4E reports differential pulsed voltammograms obtained in Z-EBs blank matrix in the presence of increasing concentrations of BPA; the relative calibration curve is reported in Fig. 4F (green line). As expected a lower sensitivity was obtained (7.22 ± 0.12 μA cm^{-2} μM^{-1}) in comparison with the calibration in PB. Also in this condition, a satisfactory nanomolar LOD was achieved (58 nM /13 μg L^{-1}) together with very high reproducibility (0.510 ± 0.008 μA μM^{-1}; RSD = 1.7 %, n = 3). In this case, the accuracy of the proposed sensing strategy was investigated by spiking BPA at 2, 20, and 200 mg L^{-1} (corresponding to 8.76, 87.61, and 876.08 μM), in agreement with the levels found in the *Z*-EBs at the end of the exposure studies (see Section 3.4). Satisfactory recoveries ranging between 94.4 and 118.4 % were obtained, with acceptable reproducibility (RSD ≤ 8.4 %, n = 3). These results are very interesting since BPA fortification was performed on the pristine zebrafish embryos (Z-EBs at 96 hpf), thereby validating the accuracy of the entire analytical procedure, which encompasses 'BPA extraction protocol from Z-EBs (Section 2.7) and the Algae paper electroanalysis (Section 2.8).

Overall, the accuracy and selectivity obtained by the analysis of BPA in both culture medium and Z-EBs can be attributed to the use of real blank matrices for the calibration curves; matrix-matched calibration allowed for replicating the most similar conditions of the real samples, obtaining low matrix effect (Visconti et al., 2023). The analysis of blank matrices (discussed above) gave rise to additional faradic peaks, which, however, did not overlap with the oxidation peak of BPA. The BPA peak resolution and identification were achieved through the high electrocatalytic activity of the Algae sensor toward BPA, ensuring the formation of a sharp and well-resolved peak.

It is important to say that the main objective of this work was to demonstrate the ability to determine the BPA accumulated by *Z*-EBs and quantify it with our sensor, under highly controlled conditions and free from potential sources of environmental and anthropic interferents, intended as structural analogues of BPA and potential chemical compounds present in real aquatic matrices.

Therefore, for the sake of clarity, the use of these sensors for the determination of BPA, to be extended to the analysis of Z-EBs grown in uncontrolled environmental waters, needs to be studied on a case-by-case basis, evaluating the sensor's ability to work in that specific type of environmental medium and to be able to determine BPA in the presence of specific potential interferents present therein.

For the sake of clarity, it should be noted that the Algae paper sensor is unsuitable for running consecutive measures in real matrices; this limitation is due to the passivation of the electrode surface (Ghanam et al., 2017). This drawback is overcome by the robustness of the manufacturing method, which allows to obtain reproducible low-impact devices via an affordable in-series fabrication approach, giving rise to sensors ready to use.

3.4. Algae paper as point-of-need device for Z-EBs exposure studies

Algae paper sensors were then used as a *point-of-need* device for exposure studies conducted in *Z*-EBs in vivo model, monitoring BPA level in culture medium at different times and BPA concentration in Z-EBS at the end of the study (96 hpf); exposure studies and electrochemical measurement are detailed in Section 2.7 and Section 2.8, respectively.

In brief, newly fertilized eggs (0 hpf) were exposed to different concentrations of BPA (0.5, 1, 2, 4, and 8 mg L^{-1}; corresponding to 2.19, 4.38, 8.76, 17.52, 35.04 μM) up to 96 hpf. BPA levels were selected to induce sub-lethal alterations (Vremere et al., 2022) according to guidelines for the testing of chemicals (OECD TG236), referring to the Fish Embryo Acute Toxicity Test (FET) guidelines (OECD, 2013). The monitoring of the BPA level during the exposure period was conducted in a semi-static and static approach; in the first case the culture medium was refreshed daily, and in the other, it was never renewed. These two exposure methods simulate different pollution release scenarios in aquatic ecosystems, i.e., discrete and continuous. Algae paper measures were performed at 4/12 h (semi-static) and 24 h (static) intervals along the 96 hpf. Fig. 5A (semi-static) and B (static) report the bisphenol-A concentration obtained (BPA_{MC}).

Interestingly, in all the cases the measured BPA concentrations (BPA_{MC}) resulted reproducible (RSD ≤ 8.4 %, $n = 3$) and in line with the nominal BPA amount (BPA_{NC}), returning a relative error between −14/+12 %, considering as true value BPA_{NC}. Noteworthy, BPA levels remained constant during time not showing significant changes in both modes (semi-static and static), proving that the BPA levels remained stable for the entire exposure period.

The Algae sensor was also used to determine BPA within the Z-EBs at the end of the exposure time (96 hpf); in-matrix calibration was used for quantification. The BPA found in Z-EBs ($BPA_{Z\text{-}EBs}$) obtained with the static approach are reported in Fig. 5C (light green bars), whereas Fig. 5D-I displays the relative raw DPV plots obtained for the different BPA levels. Fig. 5D reports the voltammogram obtained for the control *Z*-EBs group (CTRL, exposure in the absence of BPA); as expected the voltammetric profile is similar to the 'blank matrix' (see Section 3.3). In Fig. 5E-I the BPA peak centered around ~ 248 mV becomes more prominent as the concentration of BPA used in the exposure studies increases. Notably, the BPA levels found in Z-EBs resulted reproducible (RSD ≤ 8.8 %, n = 3) and significantly higher compared with the BPA nominal values (BPA_{NC}) used in the culture medium for the exposure. For this reason, the bioconcentration factor (BCF) was extrapolated using the formula $BPA_{Z\text{-}EBs}/BPA_{NC}$, intended as the concentration found in embryos ($BPA_{Z\text{-}EBs}$) with respect to 'environmental' BPA (BPA_{NC}). BCF gives quantitative information regarding the ability of a contaminant to be taken up by organisms from the water, and it is used as one of the first screening parameters for persistent, bioaccumulative, and toxic substances (Burkhard, 2021; Gómez-Regalado et al., 2023). Fig. 5C (cyan bars) indicates the BCF for *Z*-EBs subject to exposure test, highlighting an exponential trend, where values almost two orders of magnitude higher were found as a function of the BPA_{NC}. Fig. S8 reports $BPA_{Z\text{-}EBs}$ and BCF obtained for Z-EBs treated with semi-static exposure, for which a similar exponential trend was found for both parameters.

The observed BPA levels found in Z-EBS, together with the bioconcentration factors obtained, are in agreement with the literature and have been associated with different types of 'physiological' implications. In particular, exposure to 2 mg L^{-1} BPA, not cause evident effects, slight sublethal alterations are evidenced for 4 mg L^{-1}, and more severe sublethal damages were reported for 8 mg L^{-1} (Gao et al., 2022; Mu et al., 2018; Vremere et al., 2022). The sublethal alterations were probably caused by the estrogenic activity of BPA, leading to metabolic disorders and epigenetic dysfunctions with consequent developmental delay (Martínez et al., 2020; Yang et al., 2022); these aspects were not studied since out of the scope of the work. On the other hand, the observed zebrafish bioconcentration 'ability' at BPA sub-lethal levels is already reported in the literature (for embryos, larvae, and adult organisms) (Eser et al., 2022; Kim et al., 2020; Wu et al., 2017). Algaer's paper sensors point out bioconcentration phenomena starting from lower BPA levels (0.5, 1, and 2, mg L^{-1}). The adverse effects agree with the high BCF determined with the Algae sensors at 4 and 8 mg mL^{-1} BPA_{NC}, resulting in ~ 18 and ~ 43 fold higher compared to BPA_{NC}, respectively. In particular, the extremely high BCF obtained at 8 mg L^{-1} can be attributed to the presence of the chorion and the yolk sac because of the incomplete embryogenesis; the capacity of these 'organs' to strongly favor BPA bioconcentration has been reported (Duan et al., 2020).

To the best of our knowledge, this is the first study where a paper sensor was employed in BPA exposure studies with zebrafish models. Usually, chromatography methods coupled to cumbersome extraction and purification procedures are required to determine BPA in culture medium and BCF in *Z*-EBs (Eser et al., 2022; Kim et al., 2020; Mu et al., 2022; Wu et al., 2017; Yang et al., 2022; Zhao et al., 2024). Algae paper sensors ensure BPA level monitoring directly in situ, without preparation steps, providing real-time information. Algae paper sensors ensure

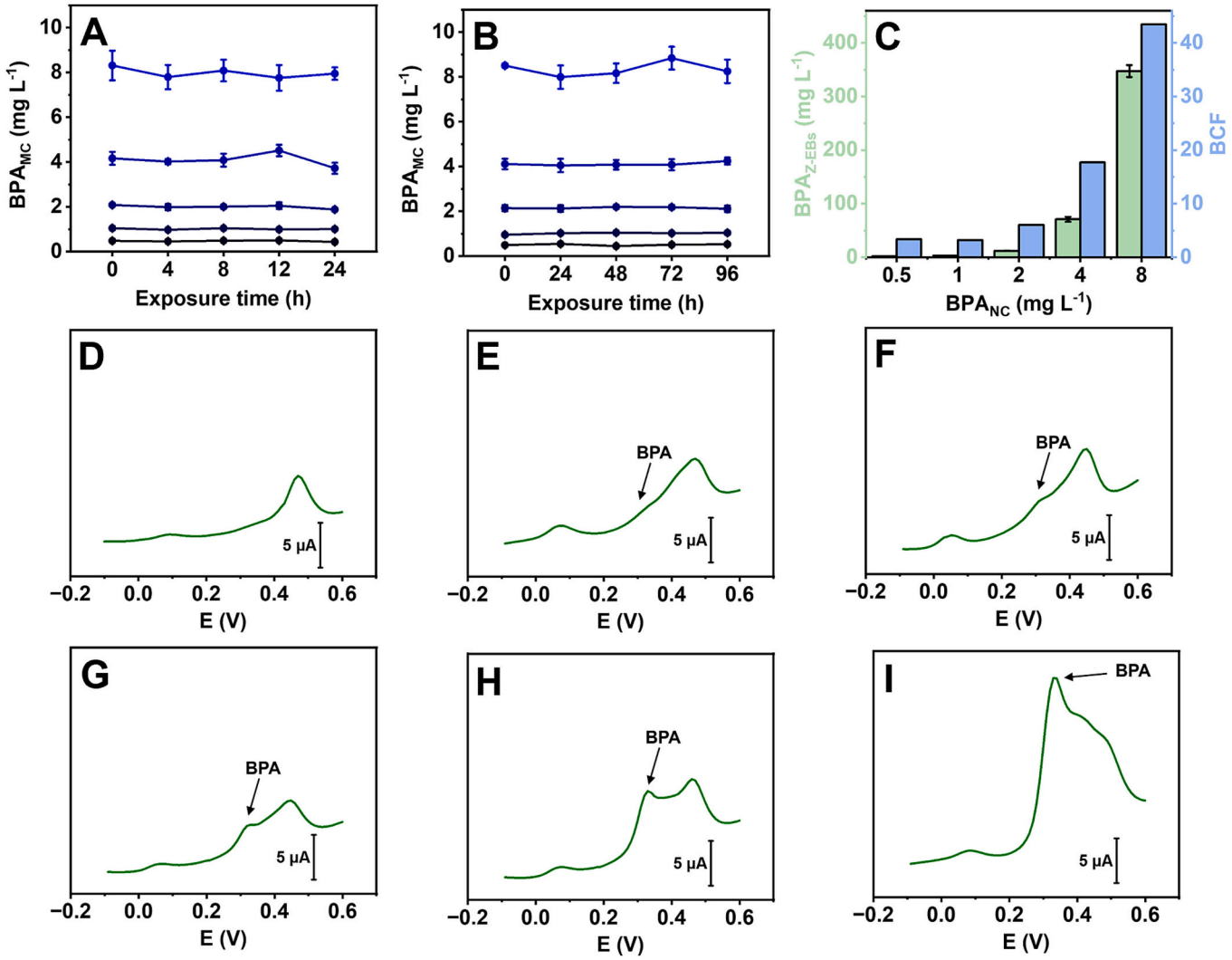

Fig. 5. BPA concentration values recorded during exposure studies in *Z*-EBs culture medium (BPA_{MC}) for the semi-static (intra-day, A) and static (inter-days, B) approach. BPA nominal concentrations (BPA_{NC}) legend: 0.5 mg L^{-1} (●), 1 mg L^{-1} (●) 2 mg L^{-1} (●), 4 mg L^{-1} (●), and 8 mg L^{-1} (●). (C) BPA found in Z-EBs ($BPA_{Z\text{-}EBs}$) and bioconcentration factor (BCF) values for each BPA_{NC} tested; data referred to static approach. Differential pulsed voltammograms obtained for the analysis of 'control Z-EBs' (CTRL, D) and BPA-exposed Z-EBs with the static approach; BPA level: (E) 0.5 mg L^{-1}, (F) 1 mg L^{-1}, (G) 2 mg L^{-1}, (H) 4 mg L^{-1}, (I) 8 mg L^{-1}.

BPA level monitoring directly in situ, without preparation steps, providing real-time information. It is fair to mention that the BPA determination, along exposure studies with Algae paper, allows requirements of the BCF guidelines, stating that the measured concentration of the tested substance should not exceed the ±20 % variation from the mean value [19]. Indeed, the algae paper allowed the BPA monitoring, both in semi-static and static approaches, in agreement with OECD TG 236 criteria (OECD, 2013), suggesting in both cases an acceptable variability (RSD $\leq$ 8.4 %, $n = 3$). In addition, the sensor proved the ability to determine BPA in Z-EBs matrix minimally treated without further 'purification'.

4. Conclusions

In this work, integrated sensors made on paper derived from seaweed biomass (Algae paper) have been proposed as affordable and effective analytical tools to assist exposure studies conducted on Z-EBs model toward the environmental contaminant BPA.

Algae paper's capability to act as a functional sensor-substrate was deeply investigated in combination with nanobiochar derived from industrial by-products, demonstrating its superior electroanalytical features in comparison with conventional paper and PET substrates. The self-standing Algae paper sensors, produced in series via a stencil-printing strategy, proved their ability to monitor BPA directly in the Z-EBs culture medium in real-time and determine the bioaccumulated BPA in Z-EBs at the end of the exposure period, ensuring accurate, robust, and selective discrimination of sublethal BPA levels. Noteworthy, Algae sensors ensure discriminating sublethal BPA levels, allowing BCF estimation.

Summing up, the marriage between a smart sensors' fabrication approach and sustainable components has led to the development of an effective electro-analytical device exploitable in exposure studies. In addition, it has been proven that the valorization of wastes and by-products may represent a valid route for the development of point-of-need devices for advanced environmental and in-vivo applications.

CRediT authorship contribution statement

Filippo Silveri: Writing – original draft, Visualization, Validation, Methodology, Investigation, Data curation, Conceptualization. **Flavio Della Pelle:** Writing – review & editing, Validation, Supervision, Project administration, Funding acquisition, Formal analysis, Conceptualization. **Carmine Merola:** Writing – review & editing, Validation, Supervision, Methodology, Investigation, Data curation, Conceptualization.

Annalisa Scroccarello: Writing – review & editing, Visualization, Validation. **Fabio Trabucco:** Writing – original draft, Methodology, Investigation. **Michele Amorena:** Writing – review & editing, Supervision, Funding acquisition. **Enrico Cozzoni:** Resources, Methodology, Investigation. **Rocco Cancelliere:** Resources, Methodology, Investigation. **Laura Micheli:** Resources, Methodology, Investigation. **Dario Compagnone:** Writing – review & editing, Validation, Supervision, Funding acquisition.

Declaration of competing interest

The authors declare that they have no known competing financial interests or personal relationships that could have appeared to influence the work reported in this paper.

Acknowledgments

This work has been funded by the European Union - NextGenerationEU, Mission 4, Component 1, under the Italian Ministry of University and Research (MUR) National Innovation Ecosystem grant ECS00000041 - VITALITY - CUP: C43C22000380007.

Appendix A. Supplementary data

Supplementary data to this article can be found online at https://doi.org/10.1016/j.scitotenv.2025.180529.

Data availability

Data will be made available on request.

References

Amalina, F., Syukor Abd Razak, A., Krishnan, S., Sulaiman, H., Zularisam, A.W., Nasrullah, M., 2022. Advanced techniques in the production of biochar from lignocellulosic biomass and environmental applications. Clean. Mater. 6, 100137. https://doi.org/10.1016/j.clema.2022.100137.

Arduini, F., 2022. Electrochemical paper-based devices: when the simple replacement of the support to print ecodesigned electrodes radically improves the features of the electrochemical devices. Curr. Opin. Electrochem. 35, 101090. https://doi.org/10.1016/j.coelec.2022.101090.

Baghel, R.S., Reddy, C., Singh, R.P., 2021. Seaweed-based cellulose applications, and future perspectives. Carbohydr. Polym. 267, 118241.

Bard, A.J., Faulkner, L.R., 2001. Electrochemical Methods: Fundamentals and Applications.

Blandón-Naranjo, L., Della Pelle, F., Vázquez, M.V., Gallego, J., Santamaría, A., Alzate-Tobón, M., Compagnone, D., 2018. Electrochemical behaviour of microwave-assisted oxidized MWCNTs based disposable electrodes: proposal of a NADH electrochemical sensor. Electroanalysis 30, 509–516. https://doi.org/10.1002/elan.201700674.

Bukhari, Q.U.A., Silveri, F., Della Pelle, F., Scroccarello, A., Zappi, D., Cozzoni, E., Compagnone, D., 2021. Water-phase exfoliated biochar nanofibers from eucalyptus scraps for electrode modification and conductive film fabrication. ACS Sustain. Chem. Eng. 9, 13988–13998. https://doi.org/10.1021/acssuschemeng.1c05893.

Burkhard, L.P., 2021. Evaluation of published bioconcentration factor (BCF) and bioaccumulation factor (BAF) data for per- and polyfluoroalkyl substances across aquatic species. Environ. Toxicol. Chem. 40, 1530–1543. https://doi.org/10.1002/etc.5010.

Cancelliere, R., Carbone, K., Pagano, M., Cacciotti, I., Micheli, L., 2019. Biochar from brewers' spent grain: a green and low-cost smart material to modify screen-printed electrodes. Biosensors 9. https://doi.org/10.3390/bios9040139.

Cancelliere, R., Rea, G., Severini, L., Cerri, L., Leo, G., Paialunga, E., Mantegazza, P., Mazzuca, C., Micheli, L., 2023. Expanding the circularity of plastic and biochar materials by developing alternative low environmental footprint sensors. Green Chem. 25, 6774–6783. https://doi.org/10.1039/d3gc01103h.

Caratelli, V., Di Meo, E., Colozza, N., Fabiani, L., Fiore, L., Moscone, D., Arduini, F., 2022. Nanomaterials and paper-based electrochemical devices: merging strategies for fostering sustainable detection of biomarkers. J. Mater. Chem. B 10, 9021–9039. https://doi.org/10.1039/d2tb00387b.

Czarny-Krzymińska, K., Krawczyk, B., Szczukocki, D., 2023. Bisphenol a and its substitutes in the aquatic environment: occurrence and toxicity assessment. Chemosphere 315. https://doi.org/10.1016/j.chemosphere.2023.137763.

Della Pelle, F., Rojas, D., Silveri, F., Ferraro, G., Fratini, E., Scroccarello, A., Escarpa, A., Compagnone, D., 2020. Class-selective voltammetric determination of hydroxycinnamic acids structural analogs using a WS2/catechin-capped AuNPs/carbon black–based nanocomposite sensor. Microchim. Acta 187, 1–13. https://doi.org/10.1007/s00604-020-04281-z.

Deroco, P.B., Junior, D.W., Kubota, L.T., 2023. Paper-based wearable electrochemical sensors a new generation of analytical devices.pdf. Electronalysis 35.

Duan, Z., Duan, X., Zhao, S., Wang, X., Wang, J., Liu, Y., Peng, Y., Gong, Z., Wang, L., 2020. Barrier function of zebrafish embryonic chorions against microplastics and nanoplastics and its impact on embryo development. J. Hazard. Mater. 395, 122621. https://doi.org/10.1016/j.jhazmat.2020.122621.

Eser, B., Tural, R., Gunal, A.C., Sepici Dincel, A., 2022. Does bisphenol A bioaccumulate on zebrafish? Determination of tissue bisphenol A level. Biomed. Chromatogr. 36. https://doi.org/10.1002/bmc.5285.

EU, 2018. Commission Regulation (EU) 2018/213 of 12 February 2018 on the use of bisphenol A in varnishes and coatings intended to come into contact with food and amending Regulation (EU) No 10/2011 as regards the use of that substance in plastic food contact materi. Off. J. Eur. Union 213, 6–12.

European Comission, 2006. Regulation (EC) 1907/2006 of the European Parliament and of teh Council of 18 December 2006 - REACH. Off. J. Eur. Union 396–849.

European Commission, 2024. Food safety – restrictions on bisphenol A (BPA) and other bisphenols in food contact materials [WWW Document]. URL. https://ec.europa.eu/info/law/better-regulation/have-your-say/initiatives/13832-Food-safety-restrictions-on-bisphenol-A-BPA-and-other-bisphenols-in-food-contact-materials_en.

Fiori, S., Scroccarello, A., Della Pelle, F., Del Carlo, M., Cozzoni, E., Compagnone, D., 2025. Integrating electrochemical sensors in circular economy: biochar-film sensors based on paper industry waste for agri-food by-product valorization. Green Anal. Chem., 100277 https://doi.org/10.1016/j.greeac.2025.100277.

Ford, A.T., Ågerstrand, M., Brooks, B.W., Allen, J., Bertram, M.G., Brodin, T., Dang, Z., Duquesne, S., Sahm, R., Hoffmann, F., Hollert, H., Jacob, S., Klüver, N., Lazorchak, J. M., Ledesma, M., Melvin, S.D., Mohr, S., Padilla, S., Pyle, G.G., Scholz, S., Saaristo, M., Smit, E., Steevens, J.A., Van Den Berg, S., Kloas, W., Wong, B.B.M., Ziegler, M., Maack, G., 2021. The role of behavioral ecotoxicology in environmental protection. Environ. Sci. Technol. 55, 5620–5628. https://doi.org/10.1021/acs.est.0c06493.

Gao, Y., Li, A., Zhang, W., Pang, S., Liang, Y., Song, M., 2022. Assessing the toxicity of bisphenol A and its six alternatives on zebrafish embryo/larvae. Aquat. Toxicol. 246, 106154. https://doi.org/10.1016/j.aquatox.2022.106154.

Ghanam, A., Lahcen, A.A., Amine, A., 2017. Electroanalytical determination of Bisphenol A: investigation of electrode surface fouling using various carbon materials. J. Electroanal. Chem. 789, 58–66. https://doi.org/10.1016/j.jelechem.2017.02.026.

Gómez-Regalado, M. del C., Martín, J., Santos, J.L., Aparicio, I., Alonso, E., Zafra-Gómez, A., 2023. Bioaccumulation/bioconcentration of pharmaceutical active compounds in aquatic organisms: assessment and factors database. Sci. Total Environ. 861. https://doi.org/10.1016/j.scitotenv.2022.160638.

Hernández-Rodríguez, J.F., Della Pelle, F., Rojas, D., Compagnone, D., Escarpa, A., 2020. Xurography-enabled thermally transferred carbon nanomaterial-based electrochemical sensors on polyethylene terephthalate-ethylene vinyl acetate films. Anal. Chem. 92, 13565–13572. https://doi.org/10.1021/acs.analchem.0c03240.

Kay, R., Desmulliez, M., 2012. A review of stencil printing for microelectronic packaging. Solder. Surf. Mt. Technol. 24, 38–50. https://doi.org/10.1108/09540911211198540.

Khabib, M.N.H., Sivasanku, Y., Lee, H.B., Kumar, S., Kue, C.S., 2022. Alternative animal models in predictive toxicology. Toxicology 465, 153053. https://doi.org/10.1016/j.tox.2021.153053.

Kim, S.S., Hwang, K.S., Yang, J.Y., Chae, J.S., Kim, G.R., Kan, H., Jung, M.H., Lee, H.Y., Song, J.S., Ahn, S., Shin, D.S., Lee, K.R., Kim, S.K., Bae, M.A., 2020. Neurochemical and behavioral analysis by acute exposure to bisphenol a in zebrafish larvae model. Chemosphere 239, 124751. https://doi.org/10.1016/j.chemosphere.2019.124751.

Kimmel, C.B., Ballard, W.W., Kimmel, S.R., Ullmann, B., Schilling, T.F., 1995. Stages of embryonic development of the zebrafish. Dev. Dyn. 203, 253–310. https://doi.org/10.1002/aja.1002030302.

Kongkaew, S., Tubtimtong, S., Thavarungkul, P., Kanatharana, P., Chang, K.H., Abdullah, A.F.L., Limbut, W., 2022. A fabrication of multichannel graphite electrode using low-cost stencil-printing technique. Sensors 22, 1–13. https://doi.org/10.3390/s22083034.

Lambré, C., Barat Baviera, J.M., Bolognesi, C., Chesson, A., Cocconcelli, P.S., Crebelli, R., Gott, D.M., Grob, K., Lampi, E., Mengelers, M., Mortensen, A., Rivière, G., Silano, V., Steffensen, I.L., Tlustos, C., Vernis, L., Zorn, H., Batke, M., Bignami, M., Corsini, E., FitzGerald, R., Gundert-Remy, U., Halldorsson, T., Hart, A., Ntzani, E., Scanziani, E., Schroeder, H., Ulbrich, B., Waalkens-Berendsen, D., Woelfle, D., Al Harraq, Z., Baert, K., Carfì, M., Castoldi, A.F., Croera, C., Van Loveren, H., 2023. Re-evaluation of the risks to public health related to the presence of bisphenol A (BPA) in foodstuffs. EFSA J. 21. https://doi.org/10.2903/j.efsa.2023.6857.

Li, H., Liu, Y., Chen, Q., Jin, L., Peng, R., 2023. Research progress of zebrafish model in aquatic ecotoxicology. Water (Switzerland) 15. https://doi.org/10.3390/w15091735.

Liu, Y., Xue, Q., Chang, C., Wang, R., Liu, Z., He, L., 2022. Recent progress regarding electrochemical sensors for the detection of typical pollutants in water environments. Anal. Sci. 38, 55–70. https://doi.org/10.2116/analsci.21SAR12.

Martínez, R., Tu, W., Eng, T., Allaire-Leung, M., Piña, B., Navarro-Martín, L., Mennigen, J.A., 2020. Acute and long-term metabolic consequences of early developmental Bisphenol A exposure in zebrafish (Danio rerio). Chemosphere 256. https://doi.org/10.1016/j.chemosphere.2020.127080.

Mu, X., Huang, Y., Li, Xuxing, Lei, Y., Teng, M., Li, Xuefeng, Wang, C., Li, Y., 2018. Developmental effects and estrogenicity of Bisphenol A alternatives in a zebrafish embryo model. Environ. Sci. Technol. 52, 3222–3231. https://doi.org/10.1021/acs.est.7b06255.

Mu, X., Qi, S., Liu, J., Yuan, L., Huang, Y., Xue, J., Qian, L., Wang, C., Li, Y., 2022. Toxicity and behavioral response of zebrafish exposed to combined microplastic and bisphenol analogues. Environ. Chem. Lett. 20, 41–48. https://doi.org/10.1007/s10311-021-01320-w.

Ni, L., Zhong, J., Chi, H., Lin, N., Liu, Z., 2023. Recent advances in sources, migration, public health, and surveillance of Bisphenol A and its structural analogs in canned foods. Foods 12. https://doi.org/10.3390/foods12101989.

Nicholson, R.S., 1965. Theory and application of cyclic voltammetryfm measurement of electrode reaction kinetics. Anal. Chem. 37, 1351–1355. https://doi.org/10.1021/ac60230a016.

Nowak, P.M., Wietecha-Posłuszny, R., Pawliszyn, J., 2021. White analytical chemistry: an approach to reconcile the principles of green analytical chemistry and functionality. TrAC Trends Anal. Chem. 138. https://doi.org/10.1016/j.trac.2021.116223.

OECD, 2013. Test No. 236: Fish Embryo Acute Toxicity (FET) Test. OECD Guidel. Test. Chem. Sect. 2, OECD Publ. 1–22.

OECD, 2019. Test No. 203: Fish, Acute Toxicity Test 24. https://doi.org/10.1787/9789264069961-en.

Oliveira, L.C., Rocha, D.S., Silva-Neto, H.A., Silva, T.A.C., Coltro, W.K.T., 2023. Polyester resin and graphite flakes: turning conductive ink to a voltammetric sensor for paracetamol sensing. Microchim. Acta 190. https://doi.org/10.1007/s00604-023-05914-9.

Olsson, J., Toth, G.B., Albers, E., 2020. Biochemical composition of red, green and brown seaweeds on the Swedish west coast. J. Appl. Phycol. 32, 3305–3317. https://doi.org/10.1007/s10811-020-02145-w.

Pastorino, P., Prearo, M., Barceló, D., 2024. Ethical principles and scientific advancements: in vitro, in silico, and non-vertebrate animal approaches for a green ecotoxicology. Green Anal. Chem. 8. https://doi.org/10.1016/j.greeac.2024.100096.

Płotka-Wasylka, J., Mohamed, H.M., Kurowska-Susdorf, A., Dewani, R., Fares, M.Y., Andruch, V., 2021. Green analytical chemistry as an integral part of sustainable education development. Curr. Opin. Green Sustain. Chem. 31. https://doi.org/10.1016/j.cogsc.2021.100508.

Rácz, Anita, Allan, B., Dwyer, T., Thambithurai, D., Killen, S.S., 2021. Identification of individual zebrafish (*Danio rerio*): a refined protocol for VIE tagging whilst considering animal welfare and the principles of the 3rs. Animals 11.

Rochester, J.R., 2013. Bisphenol A and human health: a review of the literature. Reprod. Toxicol. 42, 132–155. https://doi.org/10.1016/j.reprotox.2013.08.008.

Sachs, J.D., Schmidt-Traub, G., Mazzucato, M., Messner, D., Nakicenovic, N., Rockström, J., 2019. Six transformations to achieve the sustainable development goals. Nat. Sustain. 2, 805–814. https://doi.org/10.1038/s41893-019-0352-9.

Sanchez-Duenas, L., Gomez, E., Larrañaga, M., Blanco, M., Goitandia, A.M., Aranzabe, E., Vilas-Vilela, J.L., 2023. A review on sustainable inks for printed electronics: materials for conductive, dielectric and piezoelectric sustainable inks. Materials (Basel) 16. https://doi.org/10.3390/ma16113940.

Schäfer, S., Buchmeier, G., Claus, E., Duester, L., Heininger, P., Körner, A., Mayer, P., Paschke, A., Rauert, C., Reifferscheid, G., Rüdel, H., Schlechtriem, C., Schröter-Kermani, C., Schudoma, D., Smedes, F., Steffen, D., Vietoris, F., 2015. Bioaccumulation in aquatic systems: methodological approaches, monitoring and assessment. Environ. Sci. Eur. 27. https://doi.org/10.1186/s12302-014-0036-z.

Şen, M., Oğuz, M., Avcı, İ., 2024. Non-toxic flexible screen-printed MWCNT-based electrodes for non-invasive biomedical applications. Talanta 268. https://doi.org/10.1016/j.talanta.2023.125341.

Sfragano, P.S., Laschi, S., Palchetti, I., 2020. Sustainable printed electrochemical platforms for greener analytics. Front. Chem. 8, 1–7. https://doi.org/10.3389/fchem.2020.00644.

Sigley, E., Kalinke, C., Crapnell, R.D., Whittingham, M.J., Williams, R.J., Keefe, E.M., Janegitz, B.C., Bonacin, J.A., Banks, C.E., 2023. Circular economy electrochemistry: creating additive manufacturing feedstocks for caffeine detection from post-industrial coffee pod waste. ACS Sustain. Chem. Eng. 11, 2978–2988. https://doi.org/10.1021/acssuschemeng.2c06514.

Silva-Neto, H.A., Duarte-Junior, G.F., Rocha, D.S., Bedioui, F., Varenne, A., Coltro, W.K.T., 2023. Recycling 3D printed residues for the development of disposable paper-based electrochemical sensors. ACS Appl. Mater. Interfaces. https://doi.org/10.1021/acsami.3c00370.

Silveri, F., Paolini, D., Della Pelle, F., Bollella, P., Scroccarello, A., Suzuki, Y., Fukawa, E., Sowa, K., Di Franco, C., Torsi, L., Compagnone, D., 2023a. Lab-made flexible third-generation fructose biosensors based on 0D-nanostructured transducers. Biosens. Bioelectron. 237, 115450. https://doi.org/10.1016/j.bios.2023.115450.

Silveri, F., Scroccarello, A., Pelle, F. Della, Del Carlo, M., Compagnone, D., 2023b. Rapid pretreatment-free evaluation of antioxidant capacity in extra virgin olive oil using a laser-nanodecorated electrochemical lab-on-strip. Food Chem. 420, 136112–136122. https://doi.org/10.1016/j.foodchem.2023.136112.

Silveri, F., Della Pelle, F., Scroccarello, A., Bollella, P., Ferraro, G., Fukawa, E., Suzuki, Y., Sowa, K., Torsi, L., Compagnone, D., 2024. Exploiting CO2 laser to boost graphite inks electron transfer for fructose biosensing in biological fluids. Biosens. Bioelectron. 263. https://doi.org/10.1016/j.bios.2024.116620.

Silveri, F., Della Pelle, F., Compagnone, D., 2025. Recent advances in sustainable strategies for the integration of nanostructured sensing surfaces in electroanalytical devices. TrAC Trends Anal. Chem. 185, 118175. https://doi.org/10.1016/j.trac.2025.118175.

Stefano, J.S., Orzari, L.O., Silva-Neto, H.A., de Ataíde, V.N., Mendes, L.F., Coltro, W.K.T., Longo Cesar Paixão, T.R., Janegitz, B.C., 2022. Different approaches for fabrication of low-cost electrochemical sensors. Curr. Opin. Electrochem. 32, 100893. https://doi.org/10.1016/j.coelec.2021.100893.

Tajik, S., Beitollahi, H., Nejad, F.G., Zhang, K., Van Le, Q., Jang, H.W., Kim, S.Y., Shokouhimehr, M., 2020. Recent advances in electrochemical sensors and biosensors for detecting bisphenol A. Sensors (Switzerland) 20, 1–18. https://doi.org/10.3390/s20123364.

Tarafdar, A., Sirohi, R., Balakumaran, P.A., Reshmy, R., Madhavan, A., Sindhu, R., Binod, P., Kumar, Y., Kumar, D., Sim, S.J., 2022. The hazardous threat of Bisphenol A: toxicity, detection and remediation. J. Hazard. Mater. 423, 127097. https://doi.org/10.1016/j.jhazmat.2021.127097.

Tonon, T., Machado, C.B., Webber, M., Webber, D., Smith, J., Pilsbury, A., Cicéron, F., Herrera-Rodriguez, L., Jimenez, E.M., Suarez, J.V., Ahearn, M., Gonzalez, F., Allen, M.J., 2022. Biochemical and elemental composition of pelagic sargassum biomass harvested across the Caribbean. Phycology 2, 204–215. https://doi.org/10.3390/phycology2010011.

Vicente, A.T., Araújo, A., Gaspar, D., Santos, L., Marques, A.C., Mendes, M.J., Pereira, L., Fortunato, E., Martins, R., 2017. Optoelectronics and bio devices on paper powered by solar cells. Nanostructured Sol. Cells. https://doi.org/10.5772/66695.

Visconti, G., Boccard, J., Feinberg, M., Rudaz, S., 2023. From fundamentals in calibration to modern methodologies: a tutorial for small molecules quantification in liquid chromatography–mass spectrometry bioanalysis. Anal. Chim. Acta 1240, 340711. https://doi.org/10.1016/j.aca.2022.340711.

Vremere, A., Merola, C., Fanti, F., Sergi, M., Perugini, M., Compagnone, D., Mikhail, M., Lorenzetti, S., Amorena, M., 2022. Oxysterols profiles in zebrafish (Danio rerio) embryos exposed to bisphenol A. Food Chem. Toxicol. 165. https://doi.org/10.1016/j.fct.2022.113166.

Wu, M., Pan, C., Chen, Z., Jiang, L., Lei, P., Yang, M., 2017. Bioconcentration pattern and induced apoptosis of bisphenol A in zebrafish embryos at environmentally relevant concentrations. Environ. Sci. Pollut. Res. 24, 6611–6621. https://doi.org/10.1007/s11356-016-8351-0.

Yang, L., Chen, P., He, K., Wang, R., Chen, G., Shan, G., Zhu, L., 2022. Predicting bioconcentration factor and estrogen receptor bioactivity of bisphenol a and its analogues in adult zebrafish by directed message passing neural networks. Environ. Int. 169, 107536. https://doi.org/10.1016/j.envint.2022.107536.

Zhang, Y., Lei, Y., Lu, H., Shi, L., Wang, P., Ali, Z., Li, J., 2021. Electrochemical detection of bisphenols in food: a review. Food Chem. 346, 128895. https://doi.org/10.1016/j.foodchem.2020.128895.

Zhao, X., Liu, Z., Zhang, Y., Pan, Y., Wang, T., Wang, Z., Li, Z., Zeng, Q., Qian, Y., Qiu, J., Mu, X., 2024. Developmental effects and lipid disturbances of zebrafish embryos exposed to three newly recognized bisphenol A analogues. Environ. Int. 189, 108795. https://doi.org/10.1016/j.envint.2024.108795.

Zheng, Y., Yu, C., Fu, L., 2023. Biochar-based materials for electroanalytical applications: an overview. Green Anal. Chem. 7. https://doi.org/10.1016/j.greeac.2023.100081.